MURAJ
Minnesota Undergraduate Research & Academic Journal
z.umn.edu/MURAJ

Modeling and Proof-of-Concept of a Blackbody-Based Calibration Method in the InfraBREAD Detector

By Shardul Rao[1,2], Stefan Knirck[2,3]
[1]School of Physics and Astronomy, University of Minnesota, [2]Fermi National Accelerator Laboratory, [3]Department of Physics, Harvard University,

Abstract: The Broadband Reflector Experiment for Axion Detection (BREAD) is an ongoing collaboration searching for the conversion of yet undiscovered axion-like dark matter particles to photons in the presence of a magnetic field. InfraBREAD, a pilot experiment realization of BREAD, uses a superconducting nanowire single photon detector (SNSPD), a high-efficiency and low-noise device, to specifically detect infrared-range photons produced by $\mathcal{O}$(eV) axion-like particles. The unique BREAD coaxial reflector setup allows for the focusing of converted signal photons to a 1 mm $\times$ 1 mm SNSPD. However, when the detector is cooled to cryogenic temperatures during operation, uneven thermal contraction of reflector components may lead to a small shift in the location of the focal spot. A novel calibration method using blackbody radiation is proposed to locate the true focal spot of the detector *in situ*. Through ray tracing simulations done in FRED Optical Engineering Software, this method is demonstrated to locate the focus to within 50 µm in the axial dimension. Additionally, it is demonstrated that the blackbody photon source used in this calibration must be at a temperature of at least 15 K to 40 K, depending on the sensitivity of the SNSPD.

1 Introduction

The nature of dark matter is one of the biggest outstanding questions in modern physics. Astrophysical observations produce plentiful evidence for dark matter's existence and indicate that it makes up about 85% of the matter content of the universe. Still, little is known about its composition other than it is non-baryonic and moved non-relativistically in the early universe [RFT80, CBG+06].

The QCD axion is a hypothetical pseudoscalar boson first proposed by Steven Weinberg and Frank Wilczek as a consequence of the Peccei-Quinn mechanism, which attempts to explain why the strong interaction simultaneously conserves charge-conjugation and parity symmetry (the "strong CP problem") [PQ77b, PQ77a, Wei78, Wil78]. Wilczek and Weinberg's axion has relatively high coupling strengths (and therefore relatively high mass of 100 keV to 1 MeV), but its existence was quickly ruled out due to lack of experimental evidence. More recent theoretical models have shown that much lighter, wave-like particles can still resolve the strong CP problem and have small couplings to Standard Model particles. Two such models are the DFSZ and KSVZ "invisible" axions [DFS81, SVZ80]. "Invisble" axions and axion-like particles (ALPs) with masses in the eV range and below are therefore also well-motivated dark matter candidates [ACG+12].

In the presence of a magnetic field and a metallic surface, ALPs can convert directly to photons. The ALP's interaction with the magnetic field induces an electric field on the surface of the conductor, which then emits a photon normal to the opposite surface of the conductor [Sik83, KHA+24], a property which motivates most axion search experiments. The Broadband Reflector Experiment for Axion Detection (BREAD) is a broadband haloscope experiment searching for this axion-to-photon conversion across a wide range of axion masses from $[10^{-3}, 1]$ eV [KHA+24].

2 The BREAD Reflector and Signal Detection

From the outside in, the InfraBREAD reflector setup (Fig. 1) consists of a hollow aluminum

outer cylinder, 201 mm in radius and 567.1 mm in height, immersed in a 4 T magnetic field. A parabolic aluminum reflector 200 mm in radius sits inside of the cylinder.

The 3-dimensional parabolic reflector inside BREAD is fashioned by starting with a 2-dimensional parabolic reflector (Fig. 2), where the turning point of the true reflector is taken to be at $(r = 0, z = 0)$ and the focus of the true reflector is taken to be at $(r = f = 400\,\text{mm}, z = 0)$. The true reflector is cut in half along the r-axis between the focus and the vertex of the parabola, again cut along the line $r = \frac{f}{2} = 200\,\text{mm}$, and revolved about the z-axis to make a 3-dimensional shape.

The reflector is then slotted inside the outer cylinder, with a 1 mm clearance between the base of the reflector and the inner wall of the cylinder. Placing the cylinder wall almost exactly along the line $r = \frac{f}{2} = 200\,\text{mm}$ axis has the effect of reflecting all of the focused converted photons to the origin (Fig. 3), where a photon detector is placed.

While the reflector setup is identical between all versions of BREAD, the photon detection system varies. This work focuses on InfraBREAD, version of BREAD which searches for $\mathcal{O}$(eV) ALPs converting to infrared photons in the 600 nm to $10\,\mu\text{m} - 30\,\mu\text{m}$ wavelength range. A superconducting nanowire single photon detector, or SNSPD (Fig. 4), is used to detect these infrared signal photons. SNSPDs are particularly suitable for use in InfraBREAD over other photon detecting devices because of their sensitivity to infrared photons and their extremely low dark count rate (about 1 dark count per day) [MVS+13, HI19]. The SNSPD used in InfraBREAD sits on a 1 mm $\times$ 1 mm square chip, which is on the underside of a 57.1 mm $\times$ 57.1 mm (2.25 in $\times$ 2.25 in) detector mount such that the chip sits at the focal spot.

As the SNSPD is a superconducting device, and to additionally minimize noise and background photon counts, the InfraBREAD reflector cavity is cooled to a temperature of 0.1 K. During the cooling process, uneven thermal contraction of the aluminum reflector may lead to a millimeter-scale shift in the sensor with respect to the focal point. Therefore, an *in situ* method for aligning the sensor to the focus to sub-millimeter precision is required.

3 Blackbody Calibration Method

A blackbody-radiation-based calibration method is proposed in order to accomplish this goal. Under this method, a "hot" blackbody emitter is placed 40mm above the expected focus and blackbody radiation is allowed to radiate into the reflector setup. Due to the geometry of the parabolic reflector, any blackbody photon travelling through the focus from above at such an angle that it hits the cylindrical wall, and then the reflector, must strike the inner cylindrical wall again exactly normally on its third reflection. Therefore, it must then follow exactly its path in reverse and pass back through the SNSPD. Blackbody photons that do not travel through the focus are understood to not possess the same path-reversal property. The SNSPD mount prevents photons from reaching the SNSPD from above by functioning as a physical obstruction. Because blackbody photons that pass through the focus are the only ones which retrace their path and pass back through the focus, it is expected that by blocking blackbody radiation above the detector, the photon count rate from below the detector will be minimized precisely when the detector is on focus.

In order to test the feasibility of this method, a scale model of the reflector and calibration setup is produced in FRED Optical Engineering Software, a 3-D optical raytracing simulation software made by Photon Engineering [Pho] (Fig. 5). For each data point collected, 10^8 possible photon paths originating from the blackbody emitter are simulated. The SNSPD and SNSPD mount are moved in small increments around the focus ($\mathcal{O}$(mm) scale and below) and the number of rays that hit the SNSPD are recorded. The sizes of the emitter, SNSPD, and SNSPD mount are all varied. The effect of these variables on the relative photon counts observed by the SNSPD are modeled as a function of the SNSPD's z position.

Two broad simulation runs are undertaken. Firstly, in order to confirm this effect on a larger scale and reduce statistical fluctuations in data, simulations are conducted with an unphysically large SNSPD and SNSPD mount. While the SNSPD is kept at a constant size, the blackbody emitter and SNSPD mount are varied in size. Then, the SNSPD and SNSPD mount are shrunk to their true scale to further explore this effect on a more realistic scale.

4 Results

4.1 Varying the Size of the Emitter and SNSPD Mount

In the first run of simulations, the SNSPD is kept at a constant size of 13.33 mm $\times$ 13.33 mm. It is also modeled as a perfect absorber at 0 tempera-

ture. The radius of the circular blackbody emitter and cylindrical SNSPD mount are varied. 10^8 possible ray paths are simulated from the emitter, the SNSPD and SNSPD mount are moved in 2 mm increments in the z direction at and around the focus, and the number of rays detected by the SNSPD at each position are recorded.

Examples of the pattern impinged on the SNSPD when it is below and at focus for a particular detector geometry are displayed in Fig. 6 and 7. A large area of very low photon counts can be seen on the absorber at focus, as opposed to a distribution of high photon counts without a clear pattern seen on the absorber off focus.

Using the naive argument of blocking blackbody counts, it is expected that the number of rays detected by the SNSPD will be minimized at the focus irrespective of the geometry of the calibration setup. However, this prediction is not consistent with simulation (Fig. 8). The location of minimum photon counts is instead consistently observed to be below the focus, with a valley present around the focus.

An explanation and model is posited in Fig. 11 for the size of the valleys around the focus. This model has two motivations: for one, from Fig. 8, the width of the valley is clearly directly proportional to the radius of the SNSPD mount, and inversely proportional to the radius of the blackbody source. Additionally, at this scale, the shape of both the emitter and SNSPD mount can be seen in the pattern of rays collected by the SNSPD (Fig. 9, 10). This further indicates that the geometry of these components have an effect on what is observed by the SNSPD.

The model in Fig. 11, which states that the top of the valley is proportional to the radii of the emitter and SNSPD mount, is only able to explain the location of the top of the valley, and offers no explanation for the location of the bottom of the valley.

Regardless of this shortcoming, the model is compared to the observed top of the valley in Table 1. While the prediction does not exactly match the observed location of the top of the valley, it is consistently off by a constant factor of roughly 6 mm in each geometrical configuration. Therefore, we are still able to derive a consistent method to locate the focus based on the geometry of the detector setup.

4.2 Shrinking to a Realistic SNSPD and Mount

In the second run of simulations, the SNSPD and SNSPD mount are shrunk to their realistic size of 1 mm × 1 mm and 57.1 mm × 57.1 mm, respectively. The emitter is taken to be circular in shape and have a radius of 0.6 times the radius of the cylindrical reflector, or roughly 120 mm. Like in the previous run of simulations, the emitter is 40 mm above the expected focal point.

Using the model derived from the earlier, unphysical setup, it is expected that we observe a valley whose top is at $z_{\text{top}} = 40\,\text{mm} * \frac{28.6\,\text{mm}}{120\,\text{mm}} = 9.5\,\text{mm}$ (taking the half-width of the SNSPD mount as r' and the radius of the emitter as R). However, we are again surprised by the results (Fig. 12, 13). Under the realistic-scale setup, the original expectation that the ratio of emitted photons detected by the SNSPD is minimized at the focus is confirmed to a resolution of 50 µm.

The drastic difference between the two runs is likely due to the proportionally much smaller SNSPD as compared to the SNSPD mount in the second run. Further work is needed to understand this difference.

4.3 Blackbody Photon Counts Observed by the SNSPD

Now knowing the ratio of emitted blackbody photons which are observed by the SNSPD, it is important to calculate the rate of blackbody photons produced by the emitter and derive a temperature range at which the emitter may be kept.

The number of photon counts detected by the SNSPD follows Poisson statistics, meaning that the uncertainty on N counts is equal to $\sqrt{N}$. The detected ratio of photons differs by at least $\Delta R = 6 \times 10^{-7}$ between the focus and 50 µm away from the focus, compared to a detection ratio of $R = 1.4 \times 10^{-6}$ at the focus (Fig. 13). The minimum total number of photons emitted by the emitter (N_B) per unit of integration time (τ) in order for the photon counts on the SNSPD 50 µm away from the focus to be outside the bounds of uncertainty of the photon counts on the SNSPD at focus is given by,

$$\begin{aligned} \tfrac{N_B}{\tau} * \Delta R &\geq \sqrt{\tfrac{N_B}{\tau} * R} \\ \tfrac{N_B}{\tau} &\geq \tfrac{1}{\tau}\tfrac{R}{\Delta R^2} = \tfrac{3.8\times10^6}{\tau} \end{aligned} \tag{1}$$

.

Using Planck's law, the number density of photons emitted between $[\lambda, \lambda + d\lambda]$ by a blackbody at temperature T per integration time τ per unit area is given by

$$n_\lambda d\lambda = \frac{8\pi\tau}{\lambda^4}(e^{\frac{hc}{k_B T\lambda}} - 1)^{-1} d\lambda \tag{2}$$

The InfraBREAD SNSPD is sensitive to photons with $\lambda \in [0.6, 10 - 30]$µm, where the exact

upper bound wavelength is unknown. The emitter is again taken to be circular in shape and have a radius of 0.6 times the radius of the cylindrical reflector, or roughly 120 mm, giving it an emitting surface area of $0.045\,\mathrm{m}^2$. Equations 1 and 2 are computed for $\tau = 1\,\mathrm{min}$, $\tau = 10\,\mathrm{min}$, and $\tau = 60\,\mathrm{min}$ across a range of temperatures and maximum SNSPD upper bound wavelengths, assuming that the focus must be resolvable to 50 µm. The results are plotted in Fig. 14. The emitter must be at least in the low $\mathcal{O}(10\,\mathrm{K})$ temperature range in order to produce enough blackbody photons to resolve the drop in photon counts at the focus to within 50 µm of the focus.

5 Conclusion

The aim of this work was to model and test a consistent method for locating the focal spot of the InfraBREAD detector that is based on emitting blackbody radiation from a "hot" blackbody emitter into the reflector cavity. This method must locate the focus to sub-millimeter precision, as the superconducting nanowire single photon detector (SNSPD) used to detect focused signal photons has an area of $1\,\mathrm{mm} \times 1\,\mathrm{mm}$. This work focused on locating the focus primarily in the z-direction. 10^8 possible ray paths were simulated from the blackbody emitter using FRED Optical Engineering Software. The geometry of the detector setup was varied as needed, the SNSPD and the mount below which the SNSPD sits were moved about the focus in the z-direction, and the number of rays that the SNSPD detected was recorded. It is expected that the number of photons detected by the SNSPD is always minimized when the detector is exactly on focus. In the first stage of this work, a model of photon counts immediately about the focus as a function of the detector geometry was produced. It was clearly demonstrated that the shape and size of experimental components, namely the blackbody emitter and the SNSPD mount, have an effect on the number and pattern of emitted rays detected by an extra-large SNSPD (which has an area of $13.33\,\mathrm{mm} \times 13.33\,\mathrm{mm}$). In the second stage of this work, when the SNSPD and SNSPD mount were shrunk to their true size, the prediction of photon counts being minimized when the SNSPD is on focus was validated.

This work showed that a blackbody-radiation-based method of finding the focus of the InfraBREAD detector *in situ* is possible to a resolution of 50 µm in the axial dimension. Verifying this result in simulation is an important step. While other calibration methods for InfraBREAD have been proposed, such as one involving using lasers to mimic the path of signal photons, the precision with which these methods must be aligned and set up make them difficult to execute *in situ*. The blackbody-based method is both relatively simple to set up and is demonstrated to work to first order in simulation. It is a promising candidate for calibrating the InfraBREAD detector in coming months.

Additionally, this work demonstrates that the circular emitter (with a radius of 120 mm) must be at a temperature of at least $\mathcal{O}(10\,\mathrm{K})$ in order to resolve the focal minimum beyond the bounds of Poisson uncertainty. The temperature limits derived in this work will be critical in realizing and implementing this calibration method in the InfraBREAD detector.

6 Acknowledgements

Special thanks to Dr. Stefan Knirck and Dr. Andrew Sonnenschein for their mentoring and advice, and to the rest of the BREAD Collaboration for their feedback over the course of this project. This manuscript has been authored by Fermi Research Alliance, LLC under Contract No. DE-AC02-07CH11359 with the U.S. Department of Energy, Office of Science, Office of High Energy Physics. This work was supported in part by the U.S. Department of Energy, Office of Science, Office of Workforce Development for Teachers and Scientists (WDTS) under the Science Undergraduate Laboratory Internships Program (SULI).

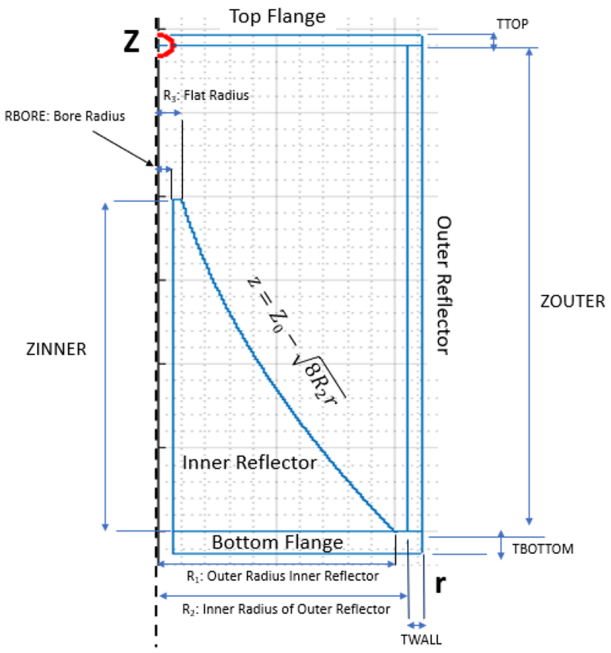

Parameter	Expression	Value [mm]	Tolerance +/- [mm]
R_1		200.0	0.2
R_2		201.00	0.05?
R_3		15.0	0.2
RBORE		25.4/2	0.2
Z_0	$\sqrt{8R_1R_2}$	567.1	-
ZINNER	$Z_0 - \sqrt{8R_2R_3}$	411.8	0.2
ZOUTER		567.10	0.05?
TWALL		25.4/4	0.2
TTOP		25.4/8	0.2
TBOTTOM		25.4/2	0.2

Figure 1: A schematic of the cross-section of half of the BREAD reflector setup, showing the dimensions of relevant components. The portion shown in the schematic is revolved a full 2π radians about the z-axis to make the three-dimensional BREAD reflector.

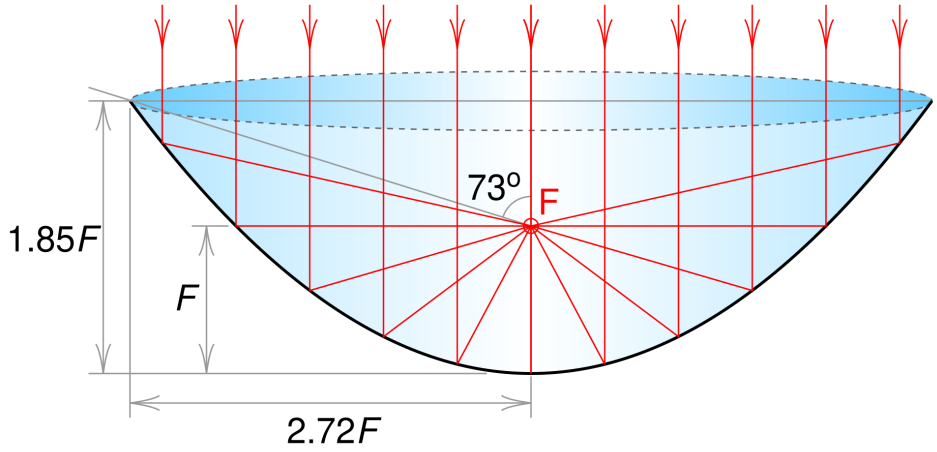

Figure 2: A true parabolic reflector focuses all incoming light that is parallel to the radial axis (henceforth the r-axis) to a single point. Image made by Wikipedia user "Cmglee" and is used under the terms of a Creative Commons Attribution-Share Alike 3.0 Unported license [CW07].

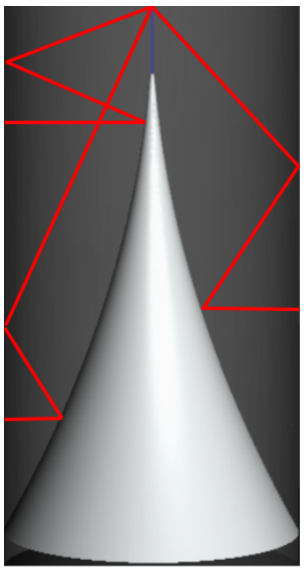

Figure 3: A cutaway view of the BREAD reflector setup, with possible paths taken by converted photons shown in red. The design of the reflector, along with the fact that converted photons are emitted perpendicularly to the inner surface of the cylinder, ensures that converted photons are focused to the detector in two reflections. Image made in FRED Optical Engineering software.

Figure 4: An image of the InfraBREAD SNSPD. A bias current is introduced across the superconducting wires of the detector. When a photon interacts with the SNSPD, superconductivity is locally broken at the interaction point and a hotspot is created, causing a measurable voltage spike.

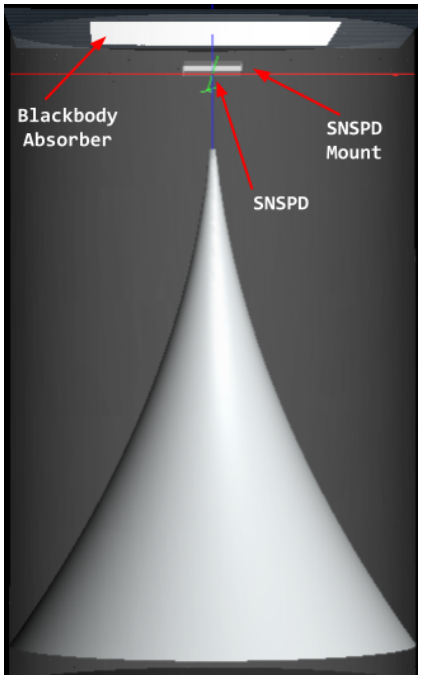

Figure 5: A scale model of the blackbody-based calibration method implemented in FRED Optical Engineering Software. The blackbody emitter, SNSPD, and SNSPD mount are labeled accordingly. Although not directly visible in the image, the SNSPD sits in the center of the bottom surface of the SNSPD mount.

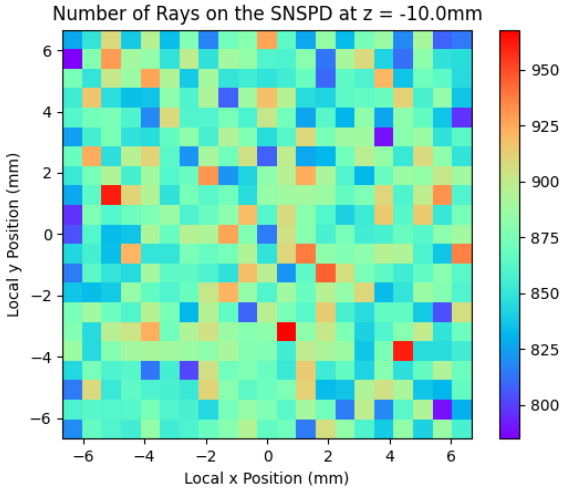

Figure 6: The pattern and number of rays detected by the 13.33 mm × 13.33 mm SNSPD when it is 10 mm below the focus for an 80 mm radius emitter and a 14 mm radius SNSPD mount.

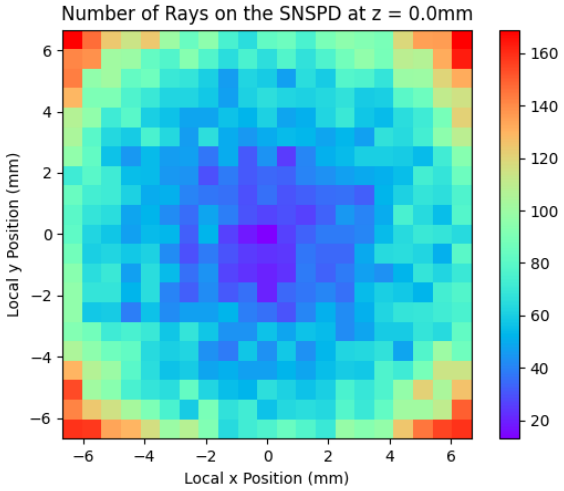

Figure 7: The pattern and number of rays detected by the 13.33 mm × 13.33 mm SNSPD when it is on focus for an 80 mm radius emitter and a 14 mm radius SNSPD mount. A circular "cold" spot can be seen on the SNSPD.

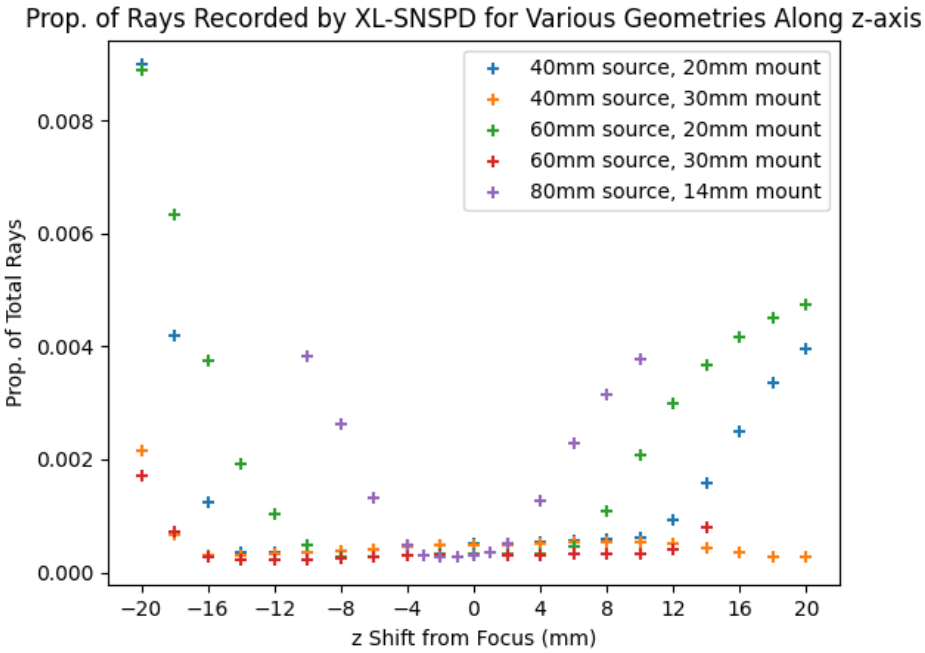

Figure 8: The ratio of total emitted rays observed by the 13.33 mm × 13.33 mm SNSPD ("XL-SNSPD") as a function of the z position of the detector. This ratio is seen to vary with the radius of the blackbody emitter ("source") and the SNSPD mount. The location of minimum photon counts is not observed at the focus but below the focus. A valley of low counts is observed around the focus with the ratio of rays detected monotonically increasing within the valley.

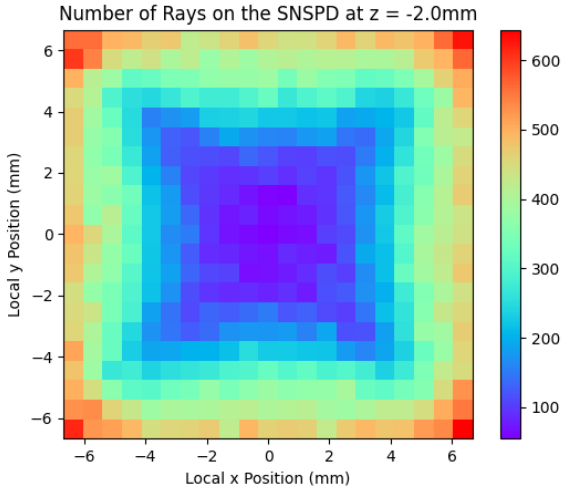

Figure 9: The pattern and number of rays detected by the 13.33 mm × 13.33 mm SNSPD when it is 2 mm below the focus. Crucially, this simulation was done with a 80 mm radius circular emitter and a square prism SNSPD mount with a basal half-width of 14 mm. The square shape of the bottom surface of the SNSPD mount can be seen as a "cold" spot on the SNSPD.

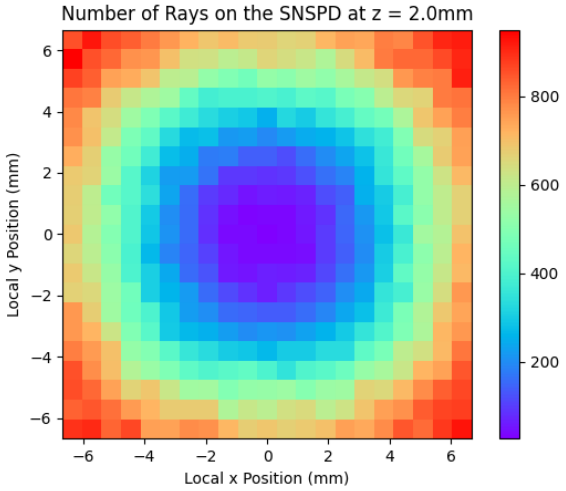

Figure 10: The pattern and number of rays detected by the 13.33 mm × 13.33 mm SNSPD when it is 2 mm above the focus. This simulation was also done with a 80 mm radius circular emitter and a square prism SNSPD mount with a basal half-width of 14 mm. The circular shape of the emitter can be seen as a "cold" spot on the SNSPD.

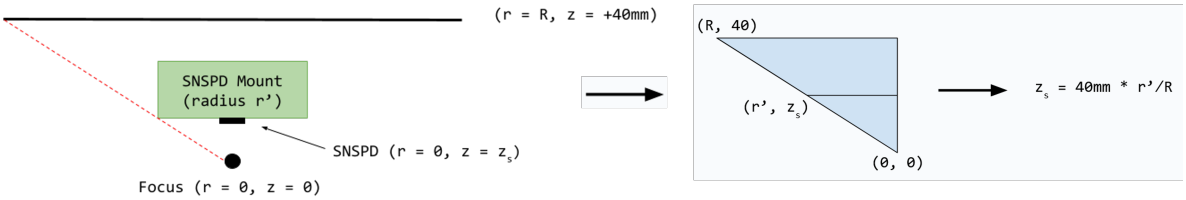

Figure 11: The z position of the "top" of the valley (z_s) is estimated to occur when all of the light from the emitter can no longer directly reach the focus. This occurs at $z_s = 40\,\text{mm} * \frac{r'}{R}$, where r' is the radius of the SNSPD mount and R is the radius of the blackbody emitter.

Source Radius, Mount Radius	Predicted Top	Observed Top
40mm, 20mm	+20mm	+14mm
40mm, 30mm	+30mm	> +20mm
60mm, 20mm	+13.3mm	+8mm
60mm, 30mm	+20mm	+14mm
80mm, 14mm	+7mm	+1mm

Table 1: Comparing the model from Fig. 11 to the observed top of the valley in Fig. 8. The top of the valley is defined as the z position at which Counts(z_{top}) / Minimum Counts ≥ 2.5. The prediction is consistently about 6mm above the observed top of the valley.

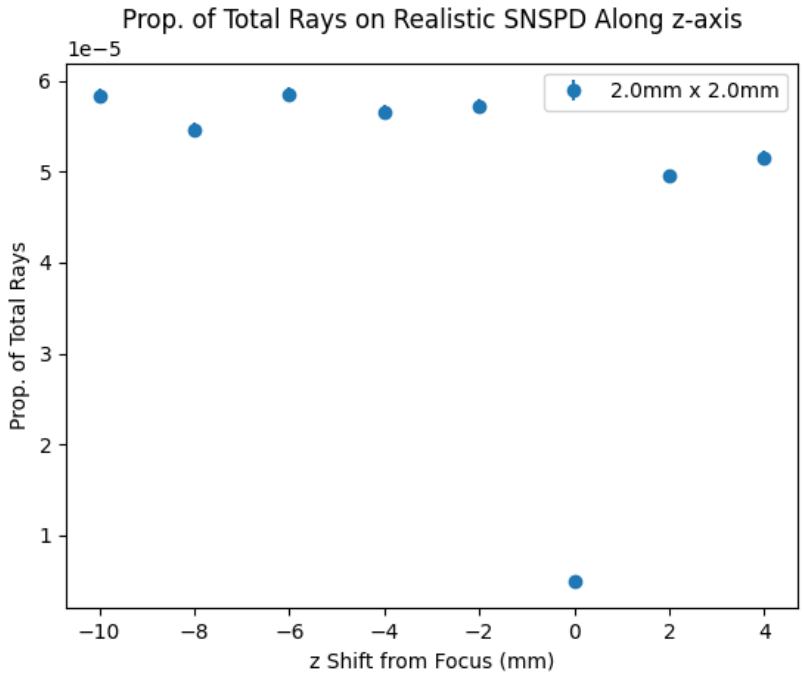

Figure 12: The ratio of total emitted rays observed by the realistically-sized SNSPD at several points along the z-axis. Unlike in Fig. 8, a clear dip in detection rate is observed at the focus. Erratum: This plot was made using photon counts on a 2 mm × 2 mm SNSPD rather than a 1 mm × 1 mm SNSPD.

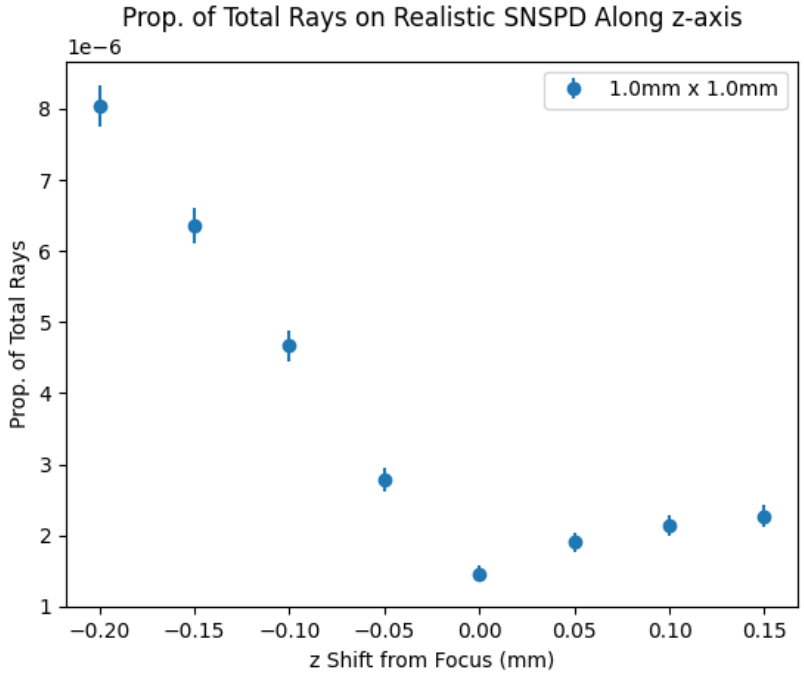

Figure 13: The ratio of total emitted rays observed by the realistically-sized SNSPD at several points along the z-axis immediately around the focus. The dip in detection rate continues to be observed at a resolution of 50 µm.

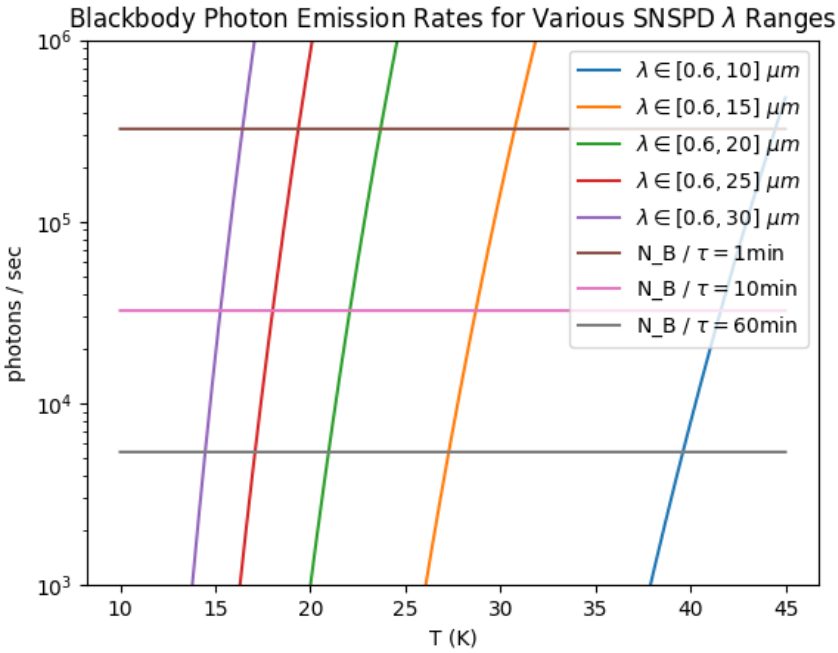

Figure 14: The rate of blackbody photons produced by a $0.045\,\mathrm{m}^2$ circular emitter between various wavelength ranges is plotted as a function of emitter temperature (calculated using Eq. 2). These wavelength ranges correspond to possible photon wavelengths observable by the SNSPD, as the exact upper bound wavelength that it is sensitive to is unknown. Also plotted is the minimum count rate needed at various integration times τ in order to be able to resolve the focal dip beyond the bounds of Poisson uncertainty to within 50 µm of the focus (Eq. 1).

References

[ACG+12] Paola Arias, Davide Cadamuro, Mark Goodsell, Joerg Jaeckel, Javier Redondo, and Andreas Ringwald. Wispy cold dark matter. *Journal of Cosmology and Astroparticle Physics*, 2012(06):013–013, June 2012.

[CBG+06] Douglas Clowe, Maruša Bradač, Anthony H. Gonzalez, Maxim Markevitch, Scott W. Randall, Christine Jones, and Dennis Zaritsky. A direct empirical proof of the existence of dark matter*. *The Astrophysical Journal*, 648(2):L109, aug 2006.

[CW07] Cmglee and WikimediaCommons. Focus-balanced parabolic reflector, 2007. File: Focus-balanced-parabolic-reflector.svg.

[DFS81] Michael Dine, Willy Fischler, and Mark Srednicki. A simple solution to the strong CP problem with a harmless axion. *Physics Letters B*, 104(3):199–202, 1981.

[HI19] Itamar Holzman and Yachin Ivry. Superconducting nanowires for single-photon detection: Progress, challenges, and opportunities. *Advanced Quantum Technologies*, 2(3–4), January 2019.

[KHA+24] Stefan Knirck, Gabe Hoshino, Mohamed H. Awida, Gustavo I. Cancelo, Martin Di Federico, Benjamin Knepper, Alex Lapuente, Mira Littmann, David W. Miller, Donald V. Mitchell, Derrick Rodriguez, Mark K. Ruschman, Matthew A. Sawtell, Leandro Stefanazzi, Andrew Sonnenschein, Gary W. Teafoe, Daniel Bowring, G. Carosi, Aaron Chou, Clarence L. Chang, Kristin Dona, Rakshya Khatiwada, Noah A. Kurinsky, Jesse Liu, Cristián Pena, Chiara P. Salemi, Christina W. Wang, and Jialin Yu. First results from a broadband search for dark photon dark matter in the 44 to 52 μeV range with a coaxial dish antenna. *Phys. Rev. Lett.*, 132:131004, Mar 2024.

[MVS+13] F. Marsili, V. B. Verma, J. A. Stern, S. Harrington, A. E. Lita, T. Gerrits, I. Vayshenker, B. Baek, M. D. Shaw, R. P. Mirin, and S. W. Nam. Detecting single infrared photons with 93% system efficiency. *Nature Photonics*, 7(3):210–214, February 2013.

[Pho] Photon Engineering. Fred optical engineering software.

[PQ77a] R. D. Peccei and Helen R. Quinn. Constraints imposed by CP conservation in the presence of pseudoparticles. *Phys. Rev. D*, 16:1791–1797, Sep 1977.

[PQ77b] R. D. Peccei and Helen R. Quinn. CP conservation in the presence of pseudoparticles. *Phys. Rev. Lett.*, 38:1440–1443, Jun 1977.

[RFT80] V. C. Rubin, Jr. Ford, W. K., and N. Thonnard. Rotational properties of 21 SC galaxies with a large range of luminosities and radii, from NGC 4605 (R=4kpc) to UGC 2885 (R=122kpc). , 238:471–487, June 1980.

[Sik83] P. Sikivie. Experimental tests of the "invisible" axion. *Phys. Rev. Lett.*, 51:1415–1417, Oct 1983.

[SVZ80] M.A. Shifman, A.I. Vainshtein, and V.I. Zakharov. Can confinement ensure natural cp invariance of strong interactions? *Nuclear Physics B*, 166(3):493–506, 1980.

[Wei78] Steven Weinberg. A new light boson? *Phys. Rev. Lett.*, 40:223–226, Jan 1978.

[Wil78] Frank Wilczek. Problem of Strong P and T Invariance in the Presence of Instantons. *Phys. Rev. Lett.*, 40:279–282, 1978.